Electronic structure of 3d transition metal pyrites MS_2 (M = Fe, Co or Ni) by analysis of the M 2p core-level photoemission spectra

1996 J. Phys.: Condens. Matter 8 2389

(http://iopscience.iop.org/0953-8984/8/14/013)

J. Phys.: Condens. Matter **8** (1996) 2389–2400. Printed in the UK

Electronic structure of 3d transition metal pyrites MS_2 (M = Fe, Co or Ni) by analysis of the M 2p core-level photoemission spectra

A E Bocquet†, K Mamiya†, T Mizokawa†, A Fujimori†, T Miyadai‡, H Takahashi§, M Môri§ and S Suga‖

† Department of Physics, University of Tokyo, Bunkyo-ku, Tokyo 113, Japan
‡ Dohto University, Junior College Division, Hiroshima-cho, Sapporo 061-11, Japan
§ Institute for Solid State Physics, University of Tokyo, Roppongi, Tokyo 106, Japan
‖ Department of Material Physics, Faculty of Engineering Science, Osaka University, Toyonaka, Osaka 560, Japan

Received 6 November 1995, in final form 19 December 1995

Abstract. We have reinterpreted the metal 2p core-level x-ray photoemission spectra of the 3d transition-metal pyrites FeS_2, CoS_2 and NiS_2 using a new version of the single-impurity cluster model which includes the effects of charge transfer to the conduction band. By accounting for the effective screening of the strong core-hole potential involving the unfilled S 3p σ^* orbitals on the ligand sites, we can successfully model the highly asymmetric lineshapes and weak satellite structures found for FeS_2 and CoS_2. Reduced screening in NiS_2 leads to the appearance of strong satellite structures and the spectrum is best interpreted using the screening channel to the narrow upper Hubbard band. These results indicate the importance of the empty ligand orbitals when interpreting the physical properties of the pyrite-type chalcogenides.

1. Introduction

The electronic structure of transition-metal (TM) dichalcogenides with the pyrite structure MS_2 (M = Fe, Co or Ni) has been of considerable interest due to the large variety in their electrical, magnetic and optical properties [1]. This variety results from the delicate interplay between the intrinsic 3d band width and the local on-site d–d correlation. For example, FeS_2 is a diamagnetic semiconductor in a low-spin state with a band gap of 0.9 eV, while CoS_2 is a ferromagnetic metal. NiS_2, on the other hand, is an antiferromagnetic insulator with a band gap of 0.3 eV which undergoes a metal–insulator transition as a function of pressure [2] or by substituting Se for S [3].

Most studies on the electronic structure of the TM pyrites have been based on a band approach [1, 4–9], and indeed the valence electronic structure of FeS_2 can be well described by band-structure calculations [7–9]. This is not the case for NiS_2, however, where electron correlations dominate over the band width. Alternatively, one can start from a localized approach as in many impurity or cluster model calculations [10–12]. Such calculations have been successful in elucidating the important electronic structure parameters in a wide range of strongly correlated TM compounds by analysis of the 2p core-level spectra obtained by x-ray photoemission spectroscopy (XPS) [11, 12]. Until recently, however, these methods have been less successful in interpreting the metal 2p core-level spectra of FeS_2 and CoS_2 due to their highly asymmetric lineshapes, reminiscent of free electron-like metals, and lack

0953-8984/96/142389+12$19.50

of distinct satellite structures [12]. These lineshapes have been qualitatively attributed to the highly polarizable nature of the $(S_2)^{2-}$ ligand which effectively screens the strong core-hole potential [8]. Local cluster methods have been more successful in interpreting the Ni 2p core-level spectra of NiS_2 [12] where electron correlation is stronger and distinct satellite structures can be found. Therefore, the 3d TM pyrites provide a challenging system for any approach to interpret their electronic structures in a consistent way.

In a recent letter [13], we have proposed a new method for introducing charge-transfer effects to empty conduction band orbitals within a local single-impurity cluster model. This approach effectively introduces non-local effects into the localized-cluster model and can account for screening by unfilled orbitals on the ligand sites and for non-local screening by empty orbitals on neighbouring TM sites. It has been successfully applied to explain the highly asymmetric lineshapes obtained for the metal 2p core-level spectra of small-gap semiconducting or metallic compounds such as NiS [14], which cannot be obtained by conventional cluster model calculations. In this work, we apply the new model to the interpretation of the metal 2p core-level spectra of the 3d TM pyrites and show quantitatively that the systematic changes in the spectra on going from FeS_2 to NiS_2 can be explained as a function of screening by the conduction band states.

The rest of the paper is organized as follows. First, we discuss the structural aspects and electronic structures of the 3d TM pyrites. After outlining the Hamiltonian and model parameters used for the calculation of the spectra, we then apply the model to reinterpret the metal 2p core-level x-ray photoemission spectra of FeS_2, CoS_2 and NiS_2. These results are compared with those obtained by conventional impurity cluster models, and various predictions and trends in the electronic structure learned from the core-level analysis are discussed.

2. Materials

FeS_2, CoS_2 and NiS_2 have a common cubic pyrite structure which can be considered as a face-centred NaCl-type array in which the anions are chalcogen atom pairs $(S_2)^{2-}$. The divalent cations are in a distorted octahedral environment with the 3d level split into a lower-lying t_{2g} triplet and a higher-lying e_g doublet. The interatomic distance within the $(S_2)^{2-}$ molecules is short due to the presence of a covalent bond, forming bonding and antibonding S 3s σ, σ^* states, and S 3p σ, σ^* and π, π^* states. The S 3p orbitals are only partially filled with ten electrons and the S 3p σ^* orbital lies above the Fermi level.

Band-structure calculations have been made for FeS_2 [4–9], CoS_2 [5–8] and NiS_2 [5–8]. All band structures show a broad band 6–7 eV wide of occupied S 3p σ, π and π^* states heavily mixed with metal 3d states. In FeS_2 these extend from about 1.5 eV to about 8.5 eV below the valence band maximum. The narrow band just below the Fermi level is the metal 3d t_{2g} level. In FeS_2, the metal 3d e_g levels are unoccupied and mix strongly with the antibonding S 3p σ^* states. The band structure predicts this compound to be a semiconductor with an indirect band gap between the Fe 3d t_{2g} and e_g states. Above the S 3p σ^* states, the next conduction band lies several electronvolts higher in energy and is of mixed metal 4sp and S 3d character [8]. With increasing atomic number from Fe to Ni, the metal 3d e_g states descend away from the S 3p σ^* states, and the hybridization between them weakens. In NiS_2 a gap of about 2 eV exists between the Ni 3d e_g and S 3p σ^* state conduction bands. The increased separation between the unoccupied metal e_g states and the S 3p σ^* states on going from FeS_2 to NiS_2 has also been observed in inverse photoemission studies [8, 15].

For FeS_2, a comparison of the predicted occupied and unoccupied band structure with the

experimental x-ray photoemission valence band spectrum [7, 8, 16, 17] and x-ray absorption spectrum [8] reveals good consistency. While the band-structure calculation gives a good description of the valence electronic structure of FeS_2, in a rigid-band picture the partially filled e_g band in CoS_2 and NiS_2 should give rise to a metallic ground state. However, CoS_2 is a ferromagnetic metal and NiS_2 is insulating, although band-structure calculations predict both to be metals [5–8]. This suggests that electron correlations become dominant on going from FeS_2 to NiS_2 and a localized viewpoint may also be valid for discussing the electronic structure.

3. Results and discussion

3.1. Calculational methods

In order to describe the core-level spectra we use a single-impurity cluster model including the presence of an unfulled conduction band. The model, based on earlier single-impurity cluster models [12, 18, 19], has been described in more detail elsewhere [13, 14], and the reader is referred to [14] for calculational details. In the cluster approximation, we consider an idealized structure with the central TM cation surrounded by an octahedron of S_2 molecules and where the band widths of the valence and conduction bands are collapsed to zero and are considered as single energy levels for simplicity. Charge transfer between the d-electron site and the valence and conduction band levels produces configurations such as $d^{n+1}\underline{L}$, $d^{n+2}\underline{L}^2$, ..., $d^{n-1}C$, $d^{n-2}C^2$, ..., $d^n\underline{L}C$, $d^n\underline{L}^2C^2$, ..., $d^{n+1}\underline{L}^2C$, $d^{n-1}\underline{L}C^2$, ..., etc, where $\underline{L}$ denotes a hole in an occupied ligand p orbital and C denotes an electron in the conduction band. The wavefunction for the formally d^n ground state spanned by the above configurations may be written as

$$\psi_g = \sum_{l,m} a_{l,m} |d^{n+l-m}\underline{L}^l C^m\rangle \tag{1}$$

where n is the number of d electrons, and the right-hand side is summed over the number of ligand holes $l = 0, 1, 2, \ldots, 10 - n - m$, and the number of electrons transferred to the conduction band $m = 0, 1, 2, \ldots, n + l$. Here, we define a charge-transfer energy to the conduction band as $\Delta^* = E(d^{n-1}C) - E(d^n)$ [20], and an effective coupling parameter to describe the interaction strength T^* between the central cluster d orbitals and the conduction band analogous to the transfer integral T.

The model presents us with a number of possibilities for the lowest-lying conduction band and the magnitude of Δ^*. For FeS_2 and CoS_2, the lowest-lying conduction band will be the strongly hybridized metal e_g–S 3p σ^* band formed by the upper Hubbard band and the empty S 3p σ^* orbitals on the ligand sites. Here, Δ^* can be set approximately equal to U, the energy required to transfer an electron from the lower Hubbard band to the hybridized conduction band. The strong hybridization means that electrons transferred to the conduction band will probably be transferred to empty orbitals on the ligand site, and the $d^n\underline{L}C$ configuration describes the transfer of an electron from the occupied to the unoccupied orbitals on the ligand site, via the local TM site. Here, the band gap $\Delta + \Delta^* - U$ will be equal to the charge-transfer energy Δ, and the configurations $d^{n+1}\underline{L}$ and $d^n\underline{L}C$ will be degenerate in the unhybridized ground state. This may not be the case for NiS_2 where the hybridization of the unfilled Ni 3d states and the S 3p states becomes weaker. Going from Fe to Ni, a lowering of the d bands is observed [5–8, 15] and the S 3p σ^* states move away from the Fermi level.

We now switch on the hybridization between the metal 3d orbitals and the valence and conduction band states. The slightly distorted octahedral environment around the cation

reduces the O_h symmetry to that of the S_6 space group, and values for the metal-to-ligand transfer integrals between the metal 3d and the occupied and unoccupied S 3p orbitals have been determined by a parametrized molecular orbital calculation [13, 22] using the relationships given by Harrison [23]. These values, listed in [13], reveal a large hybridization between the occupied and unoccupied orbitals of the pyrite system.

We now proceed to apply the model to reinterpret the metal 2p core-level spectra of FeS_2, CoS_2 and NiS_2. Experimental data are taken from [12]. Bulk plasmon satellites accompanying the main peak partially obscure the $2p_{1/2}$ satellite structure. For all spectra an energy-dependent Lorentzian lifetime broadening [12] was included to simulate the core hole d-electron multiplet splitting, as was a Gaussian broadening to simulate instrumental broadening.

3.2. FeS_2 and CoS_2

The experimental spectra for FeS_2 and CoS_2, shown in figures 1(*a*) and 1(*b*), respectively, display narrow main peaks with a highly asymmetric tail on the high-binding-energy side and apparently little satellite structure. As a starting point to interpret the spectra, we recalculate the simple cluster model predictions for the low-spin Fe^{2+} ($S = 0$) d^6 and Co^{2+} ($S = \frac{1}{2}$) d^7 ground-state configurations by setting the number of electrons transferred to the conduction band m in equation (1) to zero. In this case the unfilled orbitals on the ligand site are not accounted for and we only consider the intracluster configurations d^n, $d^{n+1}\underline{L}$, $d^{n+2}\underline{L}^2$, etc. Best-fit predictions yield parameter values $\Delta = 3.0$ eV, $U = 3.5$ eV and $T_\sigma = 1.7$ eV for FeS_2 and $\Delta = 2.5$ eV, $U = 4.2$ eV and $T_\sigma = 1.6$ eV for CoS_2 in accordance with previous studies [12]. While these parameter values are consistent with the general trends found for a large number of 3d TM compounds [12], the calculated spectra clearly cannot account for the large asymmetry of the main peaks [13]. Also, the satellite structures appearing 5–6 eV from the main peak are overestimated despite the small values of U used [13].

Table 1. Ground-state electronic configurations, Racah parameters B and C and best-fit parameter values for Δ, U, T_σ, Δ^* and T_σ^* for the 3d TM pyrites.

Compound	Ground-state configuration	Racah parameters (eV) B	C	Δ (eV)	U (eV)	T_σ (eV)	Δ^* (eV)	T_σ^* (eV)
FeS_2	$t_{2g}\uparrow^3\, t_{2g}\downarrow^3$	0.114	0.500	3.0	3.5	1.7	3.5	0.89
CoS_2	$t_{2g}\uparrow^3\, t_{2g}\downarrow^3\, e_g\uparrow$	0.120	0.558	2.5	4.2	1.6	4.2	0.82
NiS_2	$t_{2g}\uparrow^3\, t_{2g}\downarrow^3\, e_g\uparrow^2$	0.128	0.601	2.0	5.5	1.9	5.5	0.32

We now introduce the screening channel to the conduction band, using as a basis set the intracluster states and conduction band screened states $d^{n+l-m}\underline{L}^l C^m$ where $n = 6, 7$, $m = 0, 1, 2, 3$, $l = 0, \ldots, 5$, and $3 \leqslant n + l - m \leqslant 10$. Here, Δ^* is set to U, T^* is determined from the ratios in [13] and Δ, U and T_σ are treated as adjustable parameters. Best-fit results are shown for FeS_2 and CoS_2 in figures 1(*a*) and 1(*b*), respectively, with parameter values listed in table 1. The calculated spectra reproduce well the asymmetry of the experimental data and the absence of distinct satellite structures. Good agreement with experiment can be obtained without significantly changing the intracluster parameters used earlier. In the absence of the conduction band screened states, the $\underline{c}d^{n+1}\underline{L}$ states are stabilized with respect to the $\underline{c}d^n$ states in the final state ($\underline{c}$ indicates a core hole) by the

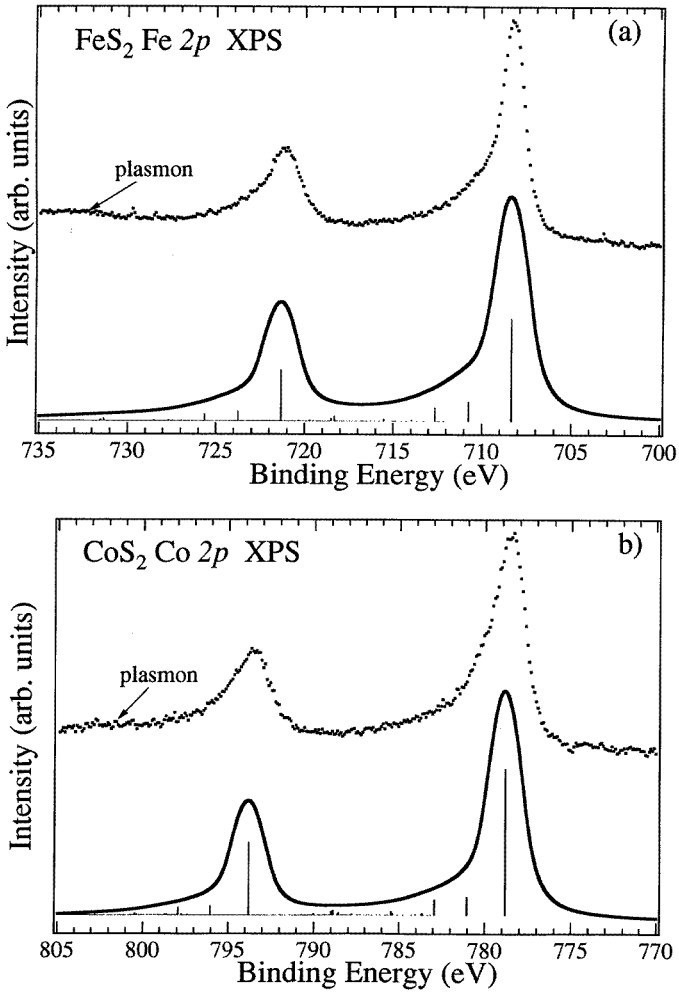

Figure 1. Experimental spectra (top curves) and calculated spectra (lower curves) for the metal 2p core levels of (*a*) FeS_2 and (*b*) CoS_2. Bulk plasmon satellites accompanying the main peaks partially obscure the $2p_{1/2}$ satellites in the experimental spectrum. Calculated spectra are obtained using a single-impurity cluster model including charge-transfer effects to the conduction band. Intracluster parameters for the calculated spectra are $\Delta = 3.0$ eV, $U = 3.5$ eV and $T_\sigma = 1.7$ eV for FeS_2 and $\Delta = 2.5$ eV, $U = 4.2$ eV and $T_\sigma = 1.6$ eV for CoS_2. Conduction band parameters are $\Delta^* = U$ and $T_\sigma^* = 0.89$ eV for FeS_2 and $\Delta^* = U$ and $T_\sigma^* = 0.82$ eV for CoS_2.

strong core hole potential, causing the appearance of strong satellite structures. However, as T_{σ^*} is relatively large in these systems (0.8–0.9 eV), much weight in the ground state will be transferred to the conduction band screened states, such as $d^n\underline{L}C$, $d^n\underline{L}^2C^2$, $d^{n+1}\underline{L}^2C$ and $d^{n+1}\underline{L}^3C^2$. Thus, despite the strong core hole potential at the d site, the lowest-energy eigenstates of these spectra are predominantly conduction band screened states, and the intracluster states such as $\underline{c}d^n$ and $\underline{c}d^{n+1}\underline{L}$ mainly contribute to the broad satellite structure. This is shown more clearly for FeS_2 in figure 2 where the major final state components of the line spectra are deconvoluted in approximately ascending order of energy. We find that

the main peak is predominantly due to conduction band screened states where one or more electrons have been transferred to the conduction bands, while the satellite features arise from less screened final states. The strong screening of the Coulomb potential reflects the large polarizability of the $(S_2)^{2-}$ ion [24, 25]. Thus, the spectra are not very sensitive to the magnitudes of the intracluster parameters Δ and U, as long as T^* is relatively large. In this case, we find similar lineshapes for different values of U and Δ within ± 1 eV.

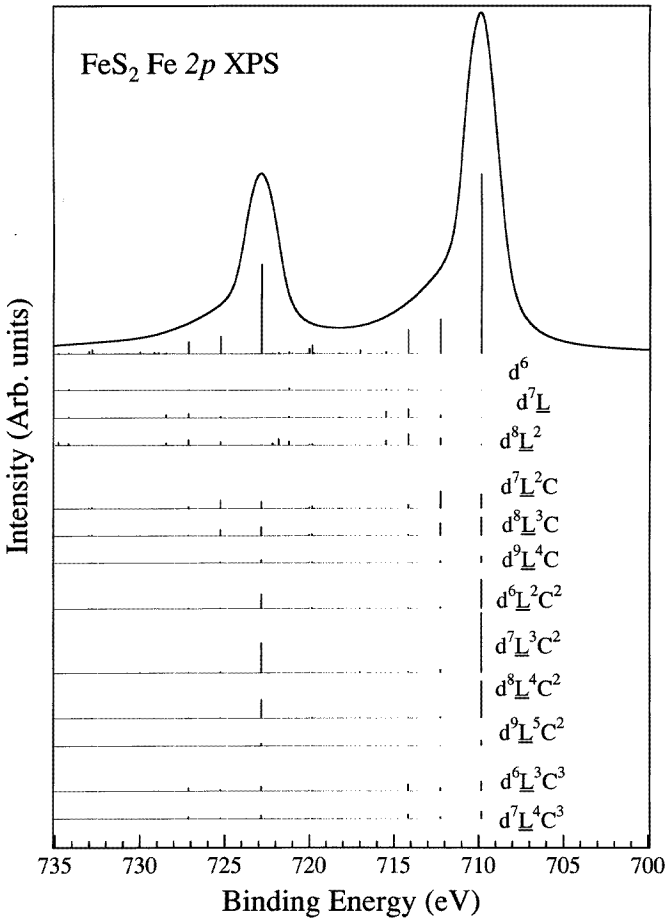

Figure 2. Major final state components for the line spectrum displayed in Figure 1(a). Components have been grouped into sets of approximately increasing energy and we have dropped the $\underline{c}$ notation for simplicity.

The degeneracy and weights of the configurations in the ground and final states for FeS_2 are listed in table 2. Here, we have grouped the configurations by the number of electrons transferred to the conduction band. In the ground state, although the lowest-energy configuration is d^6, the large value of T^* and the degeneracy of states involving a transfer of electrons from the occupied ligand orbitals to the unoccupied S 3p σ^* orbitals means that most weight is transferred to the conduction band screened states. Configurations written as $d^{6+l}\underline{L}^{m+l}C^m$ effectively describe $d^{6+l}\underline{L}^l$ states on the TM site in the presence of m electron–hole pairs on the ligand sites (similarly, configurations written as $d^{6-m}\underline{L}^l C^{m+l}$ effectively

Table 2. Configurational degeneracy and weights in the ground and final states for FeS_2 for the calculation shown in figure 2 (the $\underline{c}$ notation has been dropped for simplicity).

Configuration	Degeneracy	Ground state	Final state
d^6	1	1.0×10^{-6}	0.002
$d^7\underline{L}$	4	5.5×10^{-6}	0.008
$d^8\underline{L}^2$	6	0.1×10^{-6}	0.015
$d^9\underline{L}^3$	4	3.8×10^{-6}	0.004
$d^{10}\underline{L}^4$	1	1.2×10^{-6}	0.001
d^5C	6	29.0×10^{-6}	0.002
$d^6\underline{L}C$	25	0.001	0.026
$d^7\underline{L}^2C$	40	0.005	0.081
$d^8\underline{L}^3C$	30	0.004	0.070
$d^9\underline{L}^4C$	10	0.001	0.021
$d^{10}\underline{L}^5C$	1	48.0×10^{-6}	0.001
d^4C^2	15	0.004	0.001
$d^5\underline{L}C^2$	66	0.055	0.022
$d^6\underline{L}^2C^2$	115	0.176	0.130
$d^7\underline{L}^3C^2$	100	0.168	0.249
$d^8\underline{L}^4C^2$	45	0.052	0.157
$d^9\underline{L}^5C^2$	10	0.004	0.026
d^3C^3	20	0.001	0.000
$d^4\underline{L}C^3$	95	0.030	0.003
$d^5\underline{L}^2C^3$	186	0.160	0.030
$d^6\underline{L}^3C^3$	195	0.242	0.089
$d^7\underline{L}^4C^3$	20	0.096	0.062

describe $d^{6-m}C^m$ states in the presence of l electron–hole pairs). These electron–hole pairs provide screening of the strong core-hole potential in the final state. As the number of electron–hole pairs does not affect the d occupation at the TM site we have grouped the configurational weights by the effective number of d electrons, as shown in table 3. As expected, the d^6 states have most weight in the ground state, but there are significant contributions from the d^{n-1} and d^{n+1} states ($n = 6$), showing the importance of both the occupied and the unoccupied ligand orbitals on the ground state. This is in contrast with previous impurity models where the weights of only the $d^{n+l}\underline{L}^l$ states were considered. The effect of the core hole in the final state is to stabilize the d^{n+1} states at the expense of the d^{n-1} states. The net d-electron occupancy n_d in the ground state can be calculated from the weights shown in table 2 to be $n_d = 6.1$ [26], where the net occupations on the TM site and ligand sites can be described as $d^{6.1}\underline{L}^{0.4}C^{0.3}$. In contrast, the simple cluster model calculation of figure 1(c) yields a ground state consisting of 45% $|d^6>$, 46% $|d^7\underline{L}>$ and 8% $|d^8\underline{L}^2>$, giving $n_d = 6.6$ or $d^{6.6}\underline{L}^{0.6}$.

Finally, we discuss the convergence of the calculation with the size of the basis set. Although computational difficulties prevent the calculation of spectra for a larger basis set than that used, results for smaller basis sets are sufficiently similar to suggest that the calculation is converging. Increasing the number of electron–hole pairs used to define the conduction band screening channel increases the statistical degeneracy of the higher-energy conduction band screened states, but the proportional weight in the ground state of the various d^N ($N = n + l - m$) configurations remains largely unchanged. The spectral shape is also unlikely to vary significantly with increased basis size as it is mainly determined by the weight in the final states, which converge more rapidly due to the presence of the core hole.

Table 3. Configurational weights grouped by the effective number of d electrons.

d-electron number[a]	Ground state	Final state
3	0.001	
4	0.033	0.004
5	0.215	0.050
6	0.419	0.247
7	0.269	0.399
8	0.056	0.242
9	0.005	0.051

[a] The total number of d electrons for a $d^n\underline{L}^lC^m$ configuration is $n + l - m$.

3.3. NiS_2

The experimental Ni 2p spectrum of NiS_2 is shown in figure 3(*a*) and displays a broad, asymmetric main peak and distinct satellite structure located at 5–6 eV higher binding energies. The spectrum is similar to that of NiS [14] and asymmetric core-level lineshapes have also been observed for NiSe and NiTe [27]. The simple cluster model prediction for the high-spin d^8 ($S = 1$) configuration without the conduction band screened states is shown in figure 3(d). A best fit to the satellite intensity and position is obtained for parameters $\Delta = 2.0$ eV, $U = 5.5$ eV and $T_\sigma = 1.9$ eV, in accordance with previous studies [12]. While we can model the satellite position and intensity correctly, the large main peak asymmetry of the experimental spectrum cannot be reproduced using only this three-peak structure.

The relative success of the simple cluster model to predict the core-level spectrum of NiS_2 is due to the distinct satellite structures which suggest a significantly reduced screening of the core-hole potential by the unfilled ligand S 3p orbitals compared with the Fe and Co pyrites. Band-structure calculations also suggest a weaker hybridization, and hence weaker screening effect, between the unoccupied S 3p states and the Ni 3d states, with the S 3p σ^* states moving away from the Fermi level [5–8]. If electrons transferred to the conduction band are still considered to enter the empty ligand orbitals, Δ^* will be 3–4 eV greater than U for NiS_2 as the unfilled ligand states now lie at a higher energy than the upper Hubbard band. The reduced hybridization should also lead to a reduction in the magnitude of T^*. We can simulate the effects of reduced screening by increasing Δ^* with respect to U as shown in figure 4(a). For $\Delta^* = U$ and $T^*_\sigma/T_\sigma \approx 0.5$, we obtain a lineshape similar to the those for the Fe and Co pyrites, which is not in agreement with experiment. As Δ^* is increased, the conduction band screened states become higher in energy and the weight is shifted back to the intracluster states in the ground state, causing the appearance of strong satellite structures. This effect is further enhanced if we reduce the size of T^*. Figure 4(b) shows the effect of reducing T^* when Δ^* is set 4 eV greater than U. For a conduction band formed only by the unoccupied ligand orbitals, the best-fit result is for $\Delta^* = U + 4$ eV and $T^*_\sigma/T_\sigma \approx 0.25$ (figure 3(c)). This prediction is, however, almost identical with that of the simple cluster model above as the conduction band states now have such a high energy that they have very little weight in the ground state. Both the main peak and the satellite structures are due to intracluster states, and inclusion of the conduction band screened states provides no improvements over the previous model.

Alternatively, we can consider the lowest-lying conduction band of NiS_2 to be the narrow upper Hubbard band, as in NiS, with electrons charge transferred to the conduction band entering empty 3d orbitals on neighbouring TM sites [14]. In this scenario, Δ^* is exactly equal to U. T^* is more difficult to define as it describes the ease with which an electron can

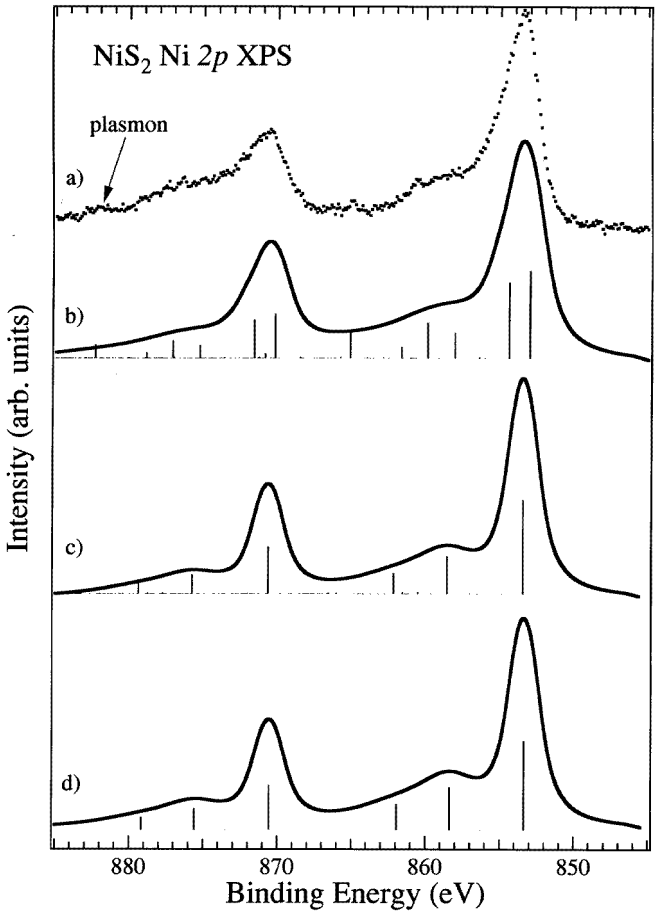

Figure 3. (*a*) Experimental and (*b*)–(*d*) calculated spectra for the Ni 2p core level of NiS_2. Calculated spectra are obtained by a single-impurity cluster model including charge-transfer effects to the conduction band where the screening channel is taken to be the narrow upper Hubbard band in (*b*), or the broad, weakly hybridized S 3p σ^* band lying at higher energy in (*c*), and a single-impurity cluster model with intracluster interactions only in (*d*). Intracluster parameters for all calculated spectra are $\Delta = 2.0$ eV, $U = 5.5$ eV and $T_\sigma = 1.9$ eV. Conduction band parameters are $\Delta^* = U$, $\delta = 4.2$ eV and $T_\sigma^* = 0.32$ eV for (*b*) and $\Delta^* = 9.5$ eV and $T_\sigma^* = 1.0$ eV for (*c*).

hop from one d site to another. Intersite hopping will be mediated by the intervening ligand orbitals and so the magnitude of T^* will also reflect the intracluster hybridization strength determined by Δ and T. Here, we must also consider the hybridization strength between the occupied S 3p orbitals and the 3d orbitals of the neighbouring TM site, which cannot be directly incorporated into a single-impurity model. This is accounted for by adding an additional hybridization correction energy δ to the energies of the $d^n\underline{L}C$, $d^n\underline{L}^2C^2$, etc, states (which describe an electron transferred from a ligand site to a neighbouring d site) which is equivalent to the hybridization splitting between the d^n and $d^{n+1}\underline{L}$ intracluster states. The band gap in the hybridized ground state is then given by $\Delta + \delta$. δ can be determined approximately by diagonalization of the Hamiltonian for a given set of parameters with T^* set to zero. We find that $\delta = 4.2$ eV for NiS_2 when $\Delta = 2.0$, $U = 5.5$ eV and $T_\sigma = 1.9$ eV.

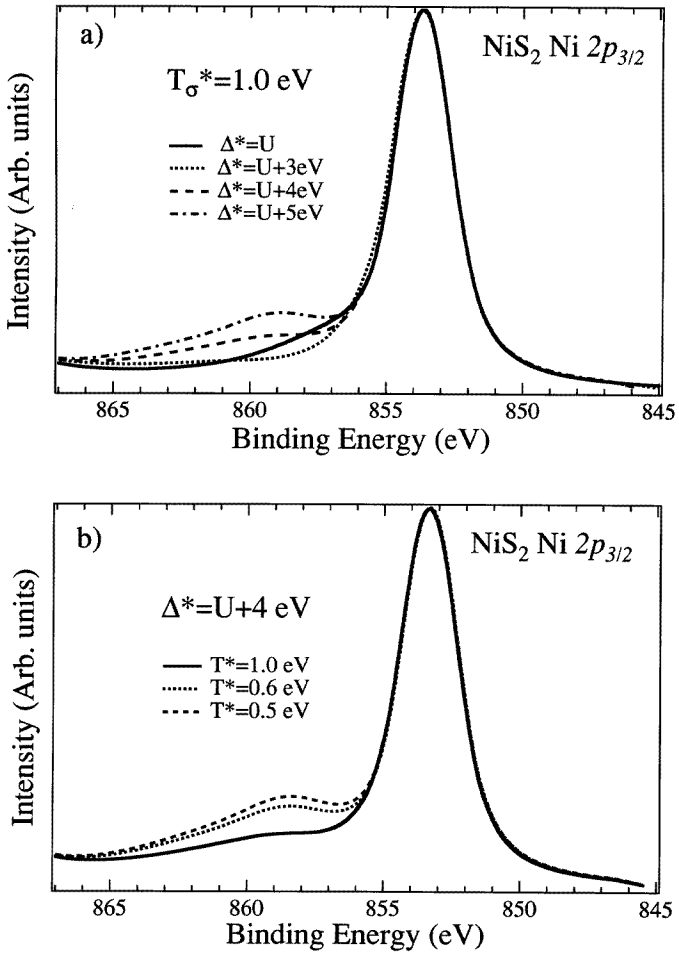

Figure 4. Calculated Ni $2p_{3/2}$ spectra for NiS_2 obtained by (a) varying Δ^* when $T^* = 1.0$ eV and (b) by varying T^* when $\Delta^* = U + 4$ eV. Here, electrons transferred to the conduction band enter the broad, weakly hybridized S 3p σ^* band. Spectra have been normalized to the height of the main peak.

Retaining the intracluster parameters found above, we introduce T^* as an adjustable parameter, including the interaction between the TM site and the conduction band. The best-fit result for $T^* = 0.32$ eV is shown in figure 3(b) where it is compared with experiment. The calculation reproduces well the large width and asymmetry of the main peak, while also correctly predicting the position and intensity of the satellite structure. Here, the weight in the ground state of the conduction band screened states is considerably reduced compared with the Fe and Co pyrites, although they contribute significantly to the additional satellite structures in the spectrum. As T^* is reduced to zero, these extra satellite structures are reduced in intensity until we return to the simple cluster model result. This calculation is equivalent to that performed for NiS with a completely filled p band in [14], and the unfilled S 3p σ^* orbitals at the ligand site are considered too high in energy to provide any additional screening.

4. Conclusions

We have applied a new version of the single-impurity cluster model, where the effects of charge transfer to the conduction band are accounted for, to reinterpret the metal 2p core-level x-ray photoemission spectra of some 3d TM pyrites. The analysis of these spectra has been difficult to achieve using previous single-impurity approaches due to their highly asymmetric lineshapes and indistinct satellite structures. The inclusion of charge-transfer screening to the strongly hybridized unfilled S 3p σ^* orbitals provides a much improved interpretation of the Fe 2p and Co 2p core-level spectra of FeS_2 and CoS_2. Here, we can accurately model the large asymmetry of the main peaks, as well as the lack of distinct satellite structures. The strength of the conduction band screened states in the ground state reflects the large polarizability of the $(S_2)^{2-}$ ligands which effectively screens the strong core-hole potential. This screening is reduced in NiS_2 as the hybridization between the unoccupied Ni 3d and S 3p states is reduced. Here, the unoccupied S 3p σ^* orbitals have too high an energy to affect significantly the predicted cluster model result and the main screening channel is due to the narrow upper Hubbard band formed by empty d orbitals on neighbouring TM sites strongly hybridized with the ligand p orbitals. Using this screening channel for electrons transferred to the conduction band, we can successfully model the Ni 2p x-ray photoemission spectrum of NiS_2, correctly predicting the large asymmetry of the main peak and the distinct satellite structures.

In conclusion we have shown that the metal 2p core-level spectra of some 3d TM pyrites can be successfully interpreted within a single-impurity model if the effects of unfilled orbitals on the ligand site are correctly accounted for. Strong screening of the core-hole potential by the unoccupied $(S_2)^{2-}$ ligand orbitals suppresses the satellite structure in FeS_2 and CoS_2, while reduced screening in NIS_2 allows the appearance of distinct satellite structures. The present analysis implies that the empty ligand states play an important role in determining the diverse properties of the pyrite-type TM compounds.

Acknowledgments

The authors would like to thank Professor D D Sarma for many helpful discussions. This work was supported by a Grant-in-Aid from the Ministry of Education, Science and Culture, Japan. One of us (AEB) gratefully acknowledges the support of the Japan Society for the Promotion of Science.

References

[1] See, e.g., Sato K 1985 *Prog. Cryst. Growth Characteristics* **11** 108, and references therein
[2] Wilson J A and Pitt G D 1971 *Phil. Mag.* **23** 1297
[3] Wilson J A 1985 *The Metallic and Non-metallic States of Matter* ed P P Edwards (London: Taylor & Francis)
[4] Khan M A 1976 *J. Phys. C: Solid State Phys.* **9** 81
[5] Bullet DW 1982 *J. Phys. C: Solid State Phys.* **15** 6163
[6] Asano S 1981 *Physical Society of Japan Meet. Abstracts* vol 3 p 154 (in Japanese)
[7] Lauer S, Trautwein A X and Harris F E 1984 *Phys. Rev.* B **29** 6774
[8] Folkerts W, Sawatzky G A, Haas C, de Groot R A and Hillebrecht F U 1987 *J. Phys. C: Solid State Phys.* **20** 4135
[9] Zeng Y and Holzwarth N A W 1994 *Phys. Rev.* B **50** 8214
[10] Zaanen J, Westra C and Sawatzky 1986 *Phys. Rev.* B **33** 8060
[11] Okada K and Kotani A 1992 *J. Phys. Soc. Japan* **61** 4619
[12] Bocquet A E, Mizokawa T, Saitoh T, Namatame H and Fujimori A 1992 *Phys. Rev.* B **46** 3771

[13] Bocquet A E, Mizokawa T, Mamiya K, Fujimori A, Matoba M, Anzai S and Suga S 1995 *J. Phys.: Condens. Matter* **7** L411
[14] Bocquet A E, Mizokawa T, Fujimori A, Matoba M and Anzai S 1995 *Phys. Rev.* B **52** 13 838
[15] Mamiya K and Fujimori A 1995 unpublished
[16] Li E K, Johnson K H, Eastman D E and Freeouf J L 1994 *Phys. Rev. Lett.* **32** 470
[17] van der Heide H, Hemmel R, van Bruggen C F and Haas C 1980 *J. Solid State Chem.* **33** 17
[18] Bocquet A E, Saitoh T, Mizokawa T and Fujimori A 1992 *Solid State Commun.* **83** 11
[19] Fujimori A, Bocquet A E, Saitoh T and Mizokawa T 1993 *J. Electron Spectrosc. Relat. Phenom.* **62** 141
[20] Fujimori A and Mizokawa T 1992 *II–VI Semiconductor Compounds* ed M Jain (Singapore: World Scientific) pp 103–30
[21] Kanamori J 1963 *Prog. Theor. Phys.* **30** 275
[22] Mamiya K 1994 *Master Thesis* University of Tokyo (in Japanese)
[23] Harrison W A 1980 *Electronic Structure and Physical Properties of Solids* (San Francisco, CA: Freeman)
[24] Suga S, Inoue K, Taniguchi M, Shin S, Seki M, Sato K and Teranishi T 1986 *J. Phys. Soc. Japan* **52** 1848
[25] Sato K 1984 *J. Phys. Soc. Japan* **53** 1617
[26] The net d-electron occupancy is calculated in the following way. For d^N configurations $d^n\underline{L}^lC^m$, the total number of d electrons is $N = n + 1 - m$. The net number of electrons transferred to the occupied ligand orbitals $n_{\underline{L}}$ is calculated from configurations where $l > m$, where from table 2 $n_{\underline{L}} = 0.269 + 2 \times 0.056 + 3 \times 0.005 = 0.396$. The net number n_C of elecrons transferred to the unoccupied conduction band orbitals is calculated from configurations where $l < m$, where from table 2 $n_C = 0.215 + 2 \times 0.033 + 3 \times 0.001 = 0.284$. The net d-electron occupancy is found from the sum of the total weights of the d^N configurations multiplied by N.
[27] Matoba M, Anzai S and Fujimori A 1992 *J. Phys. Soc. Japan* **60** 4230